Diffusional fractionation of neon isotopes in MORB melts: a molecular dynamics study

J. Nteme, M. Moreira

Supplementary Information

The Supplementary Information includes:

- Interaction Potentials and Parameters
- Numerical Modelling of Diffusion-Driven Neon Isotope Fractionation
- Tables S-1 to S-4
- Figures S-1 to S-3
- Supplementary Information References

Interaction Potentials and Parameters

The melt structure was modeled using the empirical potential developed for silicate melts of the KNCFMATS system (K_2O–Na_2O–CaO–FeO–MgO–Al_2O_3–TiO_2–SiO_2), first described by Guillot and Sator (2007) and later improved by Dufils *et al.* (2017). The interaction energy between atoms of the melt is given by a sum of pairwise contributions:

$$v(r_{ij}) = \frac{q_i\, q_j}{r_{ij}} + A_{ij}\ exp\left[-\left(\frac{r_{ij} - l_{ij}}{\lambda}\right)^2\right] + B_{ij}\ exp\left(-\frac{r_{ij}}{\rho_{ij}}\right) - \frac{C_{ij}}{r_{ij}^6}, \qquad \text{Eq. S-1}$$

where r_{ij} is the distance between atoms i and j, q_i is the effective charge of atom i. A_{ij}, l_{ij} and λ describe the covalent contribution, whereas B_{ij} and ρ_{ij} define the short-range repulsive interaction. The parameter C_{ij} corresponds to the dispersive (van der Waals) contribution. Neon atoms did not participate in any bonding interactions with the silicate network. Their interactions with the melt atoms (Si, O, Mg, Fe, etc.) were described using Lennard-Jones (LJ) potentials of the form:

$$v(r_{ij}) = 4\varepsilon\left[\left(\frac{\sigma}{r_{ij}}\right)^{12} - \left(\frac{\sigma}{r_{ij}}\right)^{6}\right] \qquad \text{Eq. S-2}$$

where ε is the depth of the Lennard–Jones potential well (i.e., the strength of the Ne–melt interaction), whereas σ is the finite-distance parameter at which the Lennard–Jones potential is zero and defines the effective size of the interacting atoms. These parameters are chosen to reproduce the weak, non-reactive nature of Ne–melt interactions, consistent with previous studies on noble gas solubility in silicate melts (Carroll and Stolper, 1993). All interaction parameters used in this study are reported in the following Tables S-1 and S-2.

Table S-1 Potential parameters for silicates (Dufils *et al.*, 2017). Values of *A*, *l, B*, *ρ* and *C* given in columns 3, 4, 5, 6, and 7, respectively, correspond to oxygen-oxygen and cation-oxygen interactions. The cation-cation interactions are described only by repulsive Coulomb forces. Note that there is no covalent interaction energy between oxygen atoms. The parameter λ in the cation-oxygen covalent energy is equal to 0.1414 Å.

	qi (e)	A (kJ/mol)	l (Å)	B (kJ/mol)	ρ (Å)	C (Å6 kJ/mol)
O	-0.945	0	0	153000	0.325	5259.83
Si	1.85	50	1.61	4869260	0.157	3036.49
Ti	1.85	32.2	1.9	5372350	0.182	9181.15
Al	1.4175	39.3	1.75	2681580	0.17	2564.84
Fe^{3+}	1.4175	40.65	1.85	1761660	0.196	7034.76
Fe^{2+}	0.945	30.2	2.05	2193830	0.194	6428.64
Mg	0.945	28.4	2	3275780	0.18	3912.7
Ca	0.945	18.6	2.4	15640400	0.179	8271.3
Na	0.4725	7.8	2.47	11937700	0.173	4673.81
K	0.4725	5.65	2.9	941307	0.242	8653.71

Table S-2 Lennard–Jones potential parameters for Ne–silicate interactions (Guillot and Sator, 2012).

	ε (kJ/mol)	σ (Å)
O	0.691	2.814
Si	7.82	1.747
Ti	8.937	2.038
Al	4.206	1.873
Fe3+	8.325	1.97
Fe2+	4.113	2.173
Mg	2.896	2.125
Ca	2.142	2.513
Na	0.984	2.6
K	0.663	3.056

Numerical Modelling of Diffusion-Driven Neon Isotope Fractionation

The diffusion coefficients obtained from the molecular dynamics simulations were subsequently used in two independent numerical calculations designed to evaluate the consequences of diffusion-driven isotope fractionation at different scales. The first calculation examines the evolution of the average isotopic composition of the melt during diffusive neon loss. The second calculation investigates the transient isotopic evolution of an individual vesicle during disequilibrium degassing. These calculations address different questions and should be viewed as complementary sensitivity analyses rather than as components of a single degassing model.

Fractionation at the melt scale

This model describes isotope fractionation associated with diffusive neon loss from the melt as a whole, treating degassing as a spatially continuous transport process toward a melt–vesicle boundary. The evolution of neon concentration in the melt is governed by the one-dimensional diffusion equation

$$\frac{\delta C}{\delta t} = D\frac{\delta^2 C}{\delta x^2} \qquad \text{Eq. S-3}$$

with an initially homogeneous concentration field, a zero-flux boundary condition at the melt interior, and a sink condition imposed at the degassing interface to represent the rapid and effectively irreversible transfer of neon into the vapor phase. The dependence of diffusivity on isotopic mass is introduced through the scaling $D(m) = D_{ref}\left(m/m_{ref}\right)^{-\beta}$, where m_{ref} = 20 g/mol and D_{ref} is the diffusion coefficient of ^{20}Ne. The governing equation is solved using a Crank–Nicolson finite-difference scheme. Spatial integration of the concentration profiles yields the cumulative fractional losses of ^{20}Ne and ^{22}Ne and the evolution of the melt-averaged normalized isotopic ratio $(^{20}Ne/^{22}Ne)/(^{20}Ne/^{22}Ne)_0$ as a function of total neon loss.

Fractionation within the vesicle

This second model focuses on the local, transient isotope fractionation that develops within an individual vesicle during disequilibrium degassing. The vesicle–melt system is represented by a spherically symmetric radial domain, consisting of a vesicle of radius a surrounded by a melt shell extending to an outer radius R. The geometry is assumed to remain constant throughout the calculation, providing a simplified framework in which the diffusion-driven component of isotope fractionation can be isolated. The model is therefore intended to evaluate the transient isotopic response of a local gas reservoir rather than to reproduce the complete evolution of a growing vesicle during magma degassing.

Neon transport in the melt is described by Fick's second law and solved numerically using an explicit finite-difference scheme. At the vesicle–melt interface, a sink boundary condition is imposed to account for the rapid and effectively irreversible transfer of neon into the vesicle, whereas a zero-flux boundary condition is applied at the outer edge of the melt domain. This formulation assumes that transfer across the melt–vesicle interface does not introduce any additional isotope fractionation, so that the overall isotopic selectivity is controlled solely by the diffusion coefficients of neon isotopes in the melt. Separate simulations are performed for ^{20}Ne and ^{22}Ne, and the vesicle-integrated neon inventories are tracked through time to calculate the transient evolution of the isotopic ratio ($^{20}Ne/^{22}Ne$) within the vesicle. The numerical solution yields isotope fractionation as a function of a dimensionless time variable, which can be subsequently rescaled using a characteristic diffusion time $\tau = (R - a)^2/D_{ref}$, where a is the vesicle radius, R is the outer radius of the melt domain, and D_{ref} is the diffusion coefficient of ^{20}Ne in the basaltic melt (7.7×10^{-10} m^2 s^{-1} at 1473 K).

The numerical implementations corresponding to these two models are provided in separate code files.

Supplementary Tables

Table S-3 Chemical composition (wt %) of the silicate (MORB) melt investigated in this study. Data are from Reynolds and Langmuir (1997). In parentheses are the numbers of cations of each species used in the simulation. The overall charge neutrality of the system is ensured by the appropriate number of oxygen atoms.

Oxides	wt %
SiO_2	50.59 (555)
TiO_2	1.52 (12)
Al_2O_3	15.11 (195)
Fe_2O_3	1.15 (9)
FeO	8.39 (78)
MgO	7.77 (126)
CaO	11.87 (141)
Na_2O	2.94 (63)
K_2O	0.13 (3)
Total	99.47

Table S-4 Diffusion coefficients of Ne pseudo-isotopes in the studied basalt melt at different temperatures and pressures.

T (K)	P (kbar)	m_{Ne} (g/mol)	D_{Ne} (10^{-9} m²/s)
1473	0	4	1.11 ± 0.05
1473	0	8	1.01 ± 0.04
1473	0	12	0.90 ± 0.04
1473	0	16	0.79 ± 0.03
1473	0	20	0.77 ± 0.04
1673	0	4	2.57 ± 0.07
1673	0	8	2.19 ± 0.07
1673	0	12	1.91 ± 0.04
1673	0	16	1.73 ± 0.05
1673	0	20	1.62 ± 0.05
1873	0	4	4.74 ± 0.11
1873	0	8	3.98 ± 0.09
1873	0	12	3.60 ± 0.08
1873	0	16	3.24 ± 0.09
1873	0	20	3.04 ± 0.07
1873	5	4	3.62 ± 0.07
1873	5	8	3.00 ± 0.05

Table S-4 continued.

T (K)	P (kbar)	m_{Ne} (g/mol)	D_{Ne} (10^{-9} m²/s)
1873	5	12	2.78 ± 0.08
1873	5	16	2.62 ± 0.05
1873	5	20	2.56 ± 0.08
1873	10	4	2.84 ± 0.05
1873	10	8	2.52 ± 0.05
1873	10	12	2.30 ± 0.05
1873	10	16	2.28 ± 0.05
1873	10	20	2.08 ± 0.07

Supplementary Figures

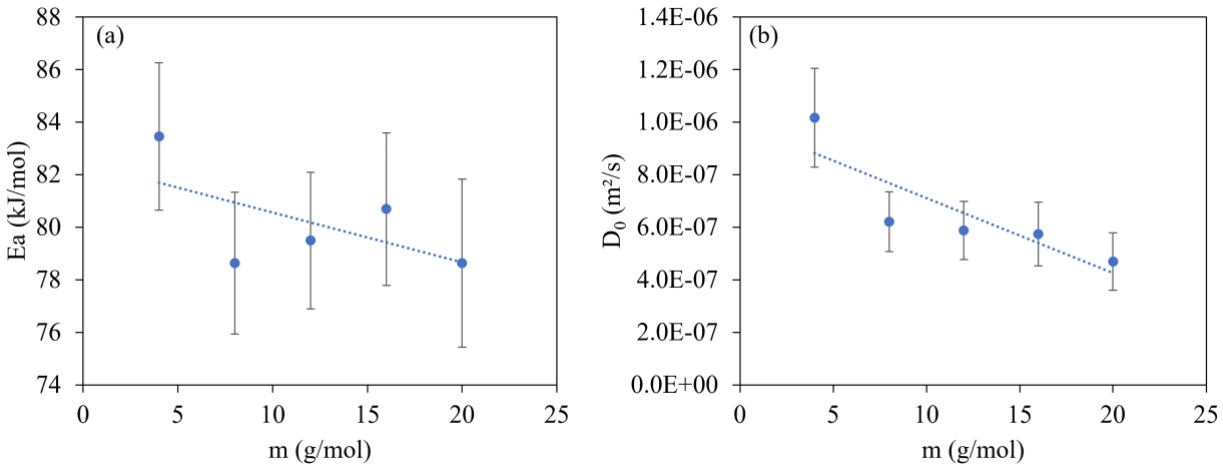

Figure S-1 Activation energy (E_a) and predicted pre-exponential factor (D_0) for Ne isotopes as a function of isotopic mass in the investigated basalt melt.

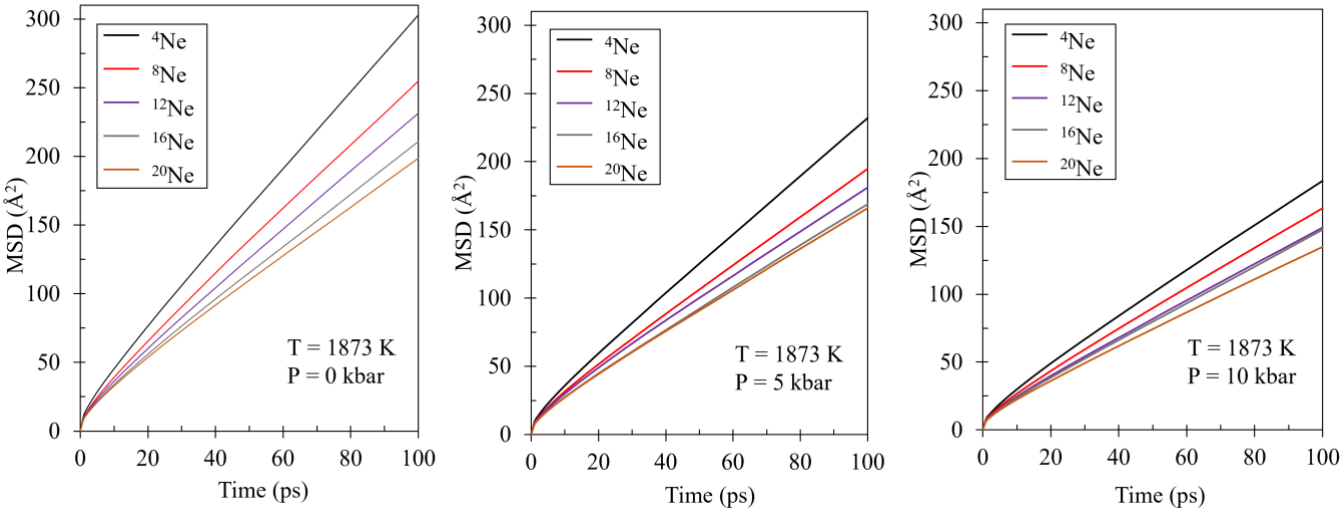

Figure S-2 Mean squared displacement (MSD) of Ne pseudo-isotopes at 1873 K under pressures of 0, 5, and 10 kbar.

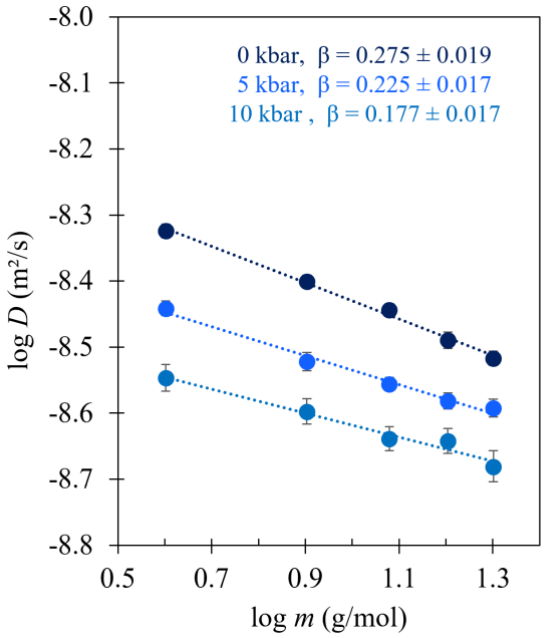

Figure S-3 Log–log plot of the diffusion coefficients of Ne pseudo-isotopes in the studied basaltic melt at 1873 K under pressures of 0, 5, and 10 kbar.

Supplementary Information References

Carroll, M.R., Stolper, E.M. (1993) Noble gas solubilities in silicate melts and glasses: New experimental results for argon and the relationship between solubility and ionic porosity. *Geochimica et Cosmochimica Acta* 57, 5039–5051. https://doi.org/10.1016/0016-7037(93)90606-W

Dufils, T., Folliet, N., Mantisi, B., Sator, N., Guillot, B. (2017) Properties of magmatic liquids by molecular dynamics simulation: the example of a MORB melt. *Chemical Geology* 461, 34–46. https://doi.org/10.1016/j.chemgeo.2016.06.030

Guillot, B., Sator, N. (2007) A computer simulation study of natural silicate melts. Part I: Low pressure properties. *Geochimica et Cosmochimica Acta* 71, 1249–1265. https://doi.org/10.1016/j.gca.2006.11.015

Guillot, B., Sator, N. (2012) Noble gases in high-pressure silicate liquids: A computer simulation study. *Geochimica et Cosmochimica Acta* 80, 51–69. https://doi.org/10.1016/j.gca.2011.11.040

Reynolds, J.R., Langmuir, C.H. (1997) Petrological systematics of the Mid-Atlantic Ridge south of Kane: Implications for ocean crust formation. *Journal of Geophysical Research: Solid Earth* 102, 14915–14946. https://doi.org/10.1029/97JB00391